environmental microbiology

Environmental Microbiology (2018) **20**(2), 546–560 doi:10.1111/1462-2920.13963

Diel regulation of photosynthetic activity in the oceanic unicellular diazotrophic cyanobacterium *Crocosphaera watsonii* WH8501

Takako Masuda, Gábor Bernát, Martina Bečková, Eva Kotabová, Evelyn Lawrenz, Martin Lukeš, Josef Komenda and Ondřej Prášil*

Centre Algatech, Opatovický mlýn, Institute of Microbiology, The Czech Academy of Sciences, Třeboň, 379 01 Czech Republic.

Summary

The oceanic unicellular diazotrophic cyanobacterium *Crocosphaera watsonii* WH8501 exhibits large diel changes in abundance of both Photosystem II (PSII) and Photosystem I (PSI). To understand the mechanisms underlying these dynamics, we assessed photosynthetic parameters, photosystem abundance and composition, and chlorophyll-protein biosynthesis over a diel cycle. Our data show that the decline in PSII activity and abundance observed during the dark period was related to a light-induced modification of PSII, which, in combination with the suppressed synthesis of membrane proteins, resulted in monomerization and gradual disassembly of a large portion of PSII core complexes. In the remaining population of assembled PSII monomeric complexes, we detected the non-functional version of the D1 protein, rD1, which was absent in PSII during the light phase. During the dark period, we also observed a significant decoupling of phycobilisomes from PSII and a decline in the chlorophyll *a* quota, which matched the complete loss of functional PSIIs and a substantial decrease in PSI abundance. However, the remaining PSI complexes maintained their photochemical activity. Thus, during the nocturnal period of nitrogen fixation *C. watsonii* operates a suite of regulatory mechanisms for efficient utilization/recycling of cellular resources and protection of the nitrogenase enzyme.

Received 22 June, 2017; revised 29 September, 2017; accepted 4 October, 2017. *For correspondence. E-mail: prasil@alga.cz; Tel. +420 384340430; Fax +420 384340415.

Introduction

Dinitrogen (N_2) fixation by marine cyanobacteria provides an important source of reduced nitrogen in tropical and subtropical oceans (Karl *et al.*, 1997) supporting 20%–40% of the total marine primary production (Lee *et al.*, 2002). However, only a few genera of bacteria contribute significantly to N_2 fixation in open oceanic environments, including filamentous cyanobacteria *Trichodesmium* (Dugdale *et al.*, 1961), unicellular diazotrophic cyanobacteria like *C. watsonii* (Zehr *et al.*, 2001; Montoya *et al.*, 2004; Moisander *et al.*, 2010) and recently discovered UCYN-A (Zehr *et al.*, 2008).

Diazotrophic cyanobacteria are the only known phototrophs containing both, a N_2 fixing system and an oxygen evolving apparatus within the same cell. However, the nitrogenase catalysing N_2 fixation is extremely sensitive to O_2 causing its irreversible inactivation (Fay, 1992; Gallon and Stal, 1992). Hence, nitrogenase activity, in principle, is incompatible with concomitant photosynthetic O_2 evolution. To solve this antagonism, the filamentous *Trichodesmium* spp. and temporally segregate nitrogen fixation from photosynthesis by activating nitrogenase in subset of cells that also contain active, although downregulated photosynthetic components (Berman-Frank *et al.*, 2001), UCYN-A protect nitrogenase by lacking oxygen evolving Photosystem II (PSII) (Zehr *et al.*, 2008), while the other unicellular diazotrophic cyanobacteria, including *C. watsonii*, temporally separate photosynthetic O_2 evolution and carbon (C) fixation from N_2 fixation, with photosynthesis occurring during the day and N_2 being fixed during the night (Tuit *et al.*, 2004; Mohr *et al.*, 2010; Dron *et al.*, 2012). The exact mechanism of this temporal separation has, however, not yet been fully elucidated (Berman-Frank *et al.*, 2003; Zehr, 2011).

Information about the diel metabolic cycle and its regulation in *C. watsonii* was acquired only recently (Church *et al.*, 2005; Mohr *et al.*, 2010; Pennebaker *et al.*, 2010; Dron *et al.*, 2012). Under 12 h/12 h light/dark (L/D) cycles, *C. watsonii* fixes N_2 during the dark phase (Tuit *et al.*, 2004; Mohr *et al.*, 2010; Dron *et al.*, 2012) while PSII activity peaks in the middle of the light period and reaches its (putative) minimum in the middle of the night (Mohr *et al.*, 2010; Pennebaker *et al.*, 2010; Rabouille and Claquin,

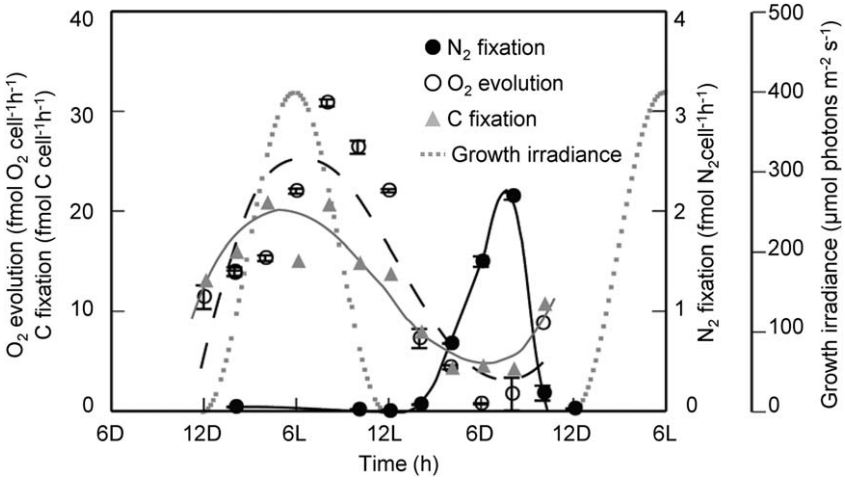

Fig. 1. Diel changes in the rate of net O_2 evolution, N_2 fixation, and potential C fixation over a 12:12 light-dark cycle of *C. watsonii*. Measurement for O_2 evolution and C fixation were conducted under 600 µmol photons m^{-2} s^{-1}. Solid black line, dashed black line and solid grey line show trend-line for N_2 fixation, O_2 evolution and C fixation respectively. Error bars are standard deviations ($n = 4$ and $n = 3$ for O_2 evolution and N_2 fixation respectively), while bell shaped dotted lines indicate the diurnal pattern of the growth irradiance.

2016). Rabouille and Claquin analysed diel changes in F_v/F_m, a measure of the photochemical quantum yield (QY) of PSII, and relative electron transfer rates through PSII (rETR), and reported a shutdown of PSII activity during the dark phase (Rabouille and Claquin, 2016). At the same time, the expression of genes encoding Photosystem I (PSI) protein subunits was suppressed (Shi *et al.*, 2010) so that the overall PSI abundance declined (Saito *et al.*, 2011). To this day, however, the diel dynamics of functional and structural changes of the photosynthetic complexes in *C. watsonii* are poorly understood.

Thus, our main objective was to determine the mechanistic underpinning responsible for the loss of PSII activity and the down-regulation of PSI during the dark phase. Understanding these dynamics in a model organism like *C. watsonnii* will provide important insight into (i) the overall regulation of N_2 fixation relative to interfering O_2 evolution and (ii) potential energetic costs of N_2 fixation.

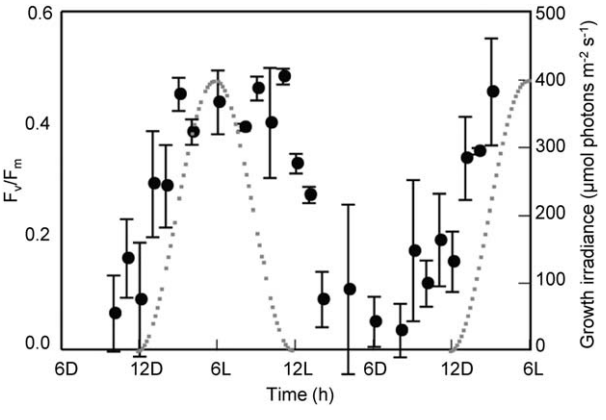

Fig. 2. Diel changes in the maximal quantum yield F_v/F_m in *C. watsonii*. Fluorescence yields were determined after 5 min exposure to weak (30 µmol photons m^{-2} s^{-1}) blue light (445 nm) whose transfer uniformly induces State 1. Error bars are standard deviations ($n = 9$); bell shaped dotted lines indicate the diurnal pattern of the growth irradiance.

Results

Diel changes in the rate of O_2 evolution, N_2 fixation and potential C fixation

Under N-deplete conditions, *C. watsonii* grew at a cell specific growth rate $\mu = 0.34 \pm 0.06$ d^{-1}. While nitrogen was fixed only during the dark phase peaking at 2.2 ± 0.0 fmol N_2 $cell^{-1}$ h^{-1} after 8 h in the dark (8D), gross O_2 evolution rates were highest during the light phase reaching a maximum of 30.8 ± 0.4 fmol O_2 $cell^{-1}$ h^{-1} at 8L and a minimum of 0.7 ± 0.1 fmol O_2 $cell^{-1}$ h^{-1} at 6D (Fig. 1). Carbon fixation rates were the highest in the middle of the light period, reaching 20.7 and 20.9 fmol C^{-1} $cell^{-1}$ h^{-1} at 4L and 8L respectively, and were minimal during the dark period with C fixation rates of 4.3 and 4.6 fmol C $cell^{-1}$ h^{-1} at 4D and 8D, respectively (Fig. 1).

Diel changes in PSII activity by variable chlorophyll fluorescence

To determine PSII photochemical activity, we measured F_v/F_m ratios during the diel cycle (Fig. 2), where F_m and F_v correspond to maximal and variable fluorescence yield, respectively (Table 1). In cyanobacteria, the process of state transitions can significantly influence fluorescence yields and as a consequence, also the value of F_v/F_m: cyanobacteria adapted to darkness are usually in State 2 and the F_v/F_m is low and *vice versa*, cells adapted to blue or white light are in State 1 and F_v/F_m is high (for recent review, see e.g., Kirilovsky *et al.*, 2015). Therefore, to minimize the possible effect of state transitions during diel measurements, we determined F_v/F_m after 5 min exposure to low-intensity blue light, when, regardless of the initial state, cells were in State 1. Diel changes in F_v/F_m followed the temporal changes with maxima ($\sim$ 0.45) at mid-day and rapidly dropping once irradiance decreased below 50 µmol photons m^{-2} s^{-1}, reaching a minimum of < 0.1

Table 1. Fluorescence parameters and their meaning.

Parameter	Meaning
F_o	Intrinsic fluorescence in the dark period
F_t	Intrinsic fluorescence in the light period
F_m	Maximum fluorescence
F_v	Variable fluorescence
	$F_v = (F_m - F_o)$ in the dark period
	$F_v = (F_m - F_t)$ in the light period
F_v/F_m	Maximum PSII efficiency
	$F_v/F_m = (F_m - F_o)/F_m$ in the dark period
	$F_v/F_m = (F_m - F_t)/F_m$ in the dark period
*P*m'max	Functional PSI content
Y(*I*)	Maximum PSI efficiency
ETR(*I*)	PSI mediated electron transport rate

around 6D (Fig. 2). During the second half of the night, F_v/F_m started to recover to up to ~ 0.15–0.2 by the start of the light period. This indicates that, regardless of its abundance, PSII is active during the light period, and is being inactivated during the night, thus matching the O_2 evolution data (Fig. 1).

To better understand the diel changes in F_v/F_m and PSII activity, we also monitored Chl fluorescence yields inside the bioreactor and observed significant changes in intrinsic Chl fluorescence yield, F_o in the dark and F_t in the light period, respectively, and the maximal fluorescence yield, F_m (Fig. 3A). These diel changes can be divided into four distinct phases (Fig. 3): Photosynthesis and growth phase, where F_t was low and almost constant during the day (i.e., from 2L to 9L) and preparation for N_2 fixation phase during which F_t and F_o started to increase rapidly at the end of the light period (after 9L) (Fig. 3A). The rise of F_t and F_o continued up to 3D, when it reached a nocturnal maximum that was about twofold higher than the diurnal steady-state value, and then gradually decreased from 3D to 2L again

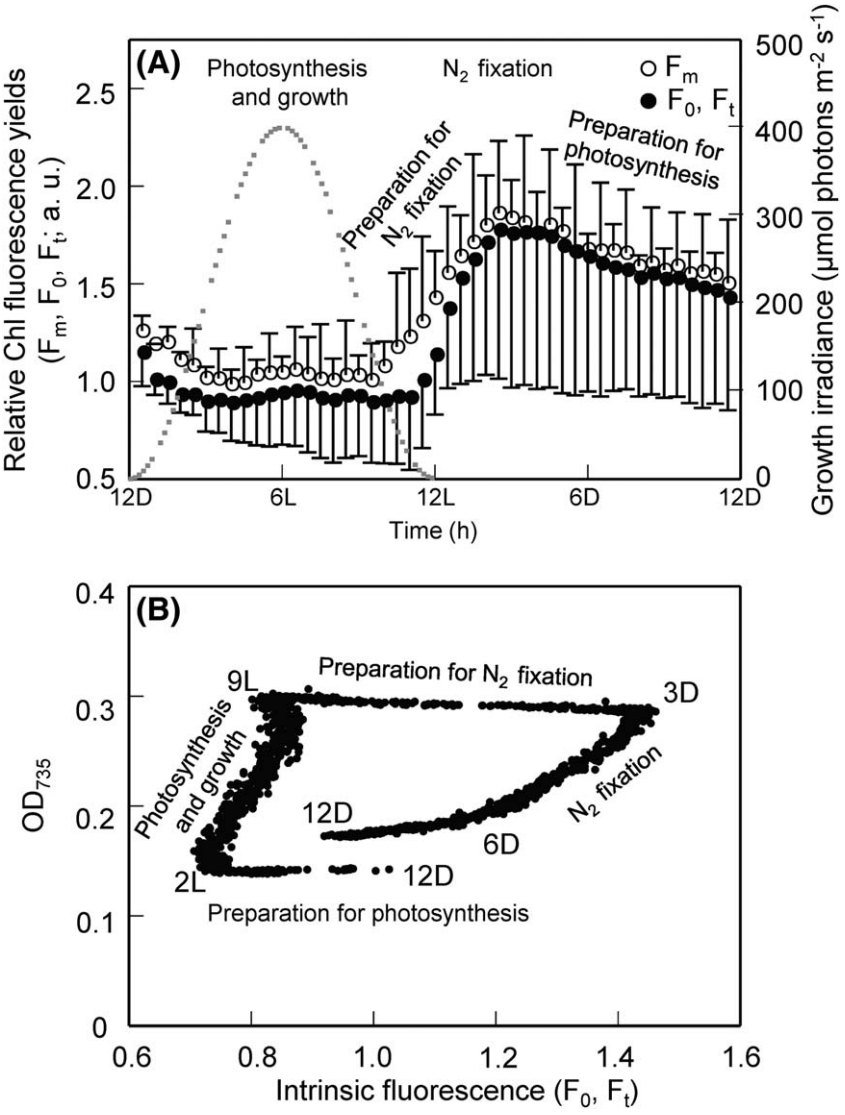

Fig. 3. Diel changes in *in situ* Chl fluorescence of *C. watsonii*. (A) Diel pattern of maximal-and minimal/intrinsic Chl fluorescence were averaged over 9 individual experiments and 7 subsequent days (63 data sets in total) and normalized to $F_t = 1.0$ at 1L. Error bars represent standard deviations, bell shaped dotted line indicates the diurnal pattern of the growth irradiance. (B) Relationship between F_t and OD at 735nm. P1–P4 denote distinctly different metabolic phases (see text for details).

during phases N_2 fixation and preparation for photosynthesis, respectively. The highest F_v values were observed at the beginning and at the end of the light period while the rise of F_t and F_o observed at the beginning of the dark period (from 11L to 3D) was accompanied by a decline in F_v (Fig. 3A). After 2D, F_v was almost negligible, that is, F_m was only slightly higher than F_o. F_v started to recover gradually during the second half of the dark period (i.e., after 6D, which separates two phases of N_2 fixation and preparation for photosynthesis) (Fig. 3A). The 4 different phases of fluorescence characteristics during the diel cycle of *C. watsonii* become even more apparent by plotting the intrinsic fluorescence against the optical density of the culture at 735 nm (OD_{735}) (Fig. 3B), which revealed the dynamics of growth, and changes in pigment to protein coupling during the four distinct phases (see Discussion).

Diel changes in PSII activity by TL

To confirm diel dynamics of PSII activity, we also used thermoluminescence (TL). TL records photons emitted during charge recombination in active PSII reaction centres. Cells are first cooled to low temperature to prevent spontaneous recombinations, then illuminated to induce charge separation and then the weak photon emission resulting from charge recombinations (the so-called glow curve) is recorded during heating of the sample in the dark. Following excitation by two single turnover flashes, TL glow curves were dominated by the so-called B band, which originates from the charge recombination between the S_2 and S_3 states of the O_2 evolving complex and reduced bound plastoquinone Q_B^- within PSII (Rutherford *et al*., 1982; Demeter and Vass, 1984) (Fig. 4A). The overall TL intensity is roughly proportional to the number of active PSII centres, which is calculated as the area under a TL glow curve. PSII abundance showed a clear diel cycle (Fig. 4B) similar to that of O_2 evolution and F_v/F_m, that is, a decline in TL intensity during the first half of the dark phase (12L–6D) and a strong increase with the beginning of the light phase (from 12D).

Fluorescence emission spectra

Spectrum of daylight (4L–8L) samples with Chl excitation at 425 nm was dominated by three emission bands peaking at 685, 693 and 715 nm (Fig. 5). Fluorescence at 685 nm (F685) can be attributed to emission from both PSII (arising from Chl in CP43 and CP47 core antenna proteins) and phycobilisome (PBS) terminal emitter. F693 represents fluorescence emission solely from active PSII (arising from Chl in CP47) (Andrizhiyevskaya *et al*., 2005, Suggett *et al*., 2009, D'Haene *et al*., 2015) while F715 stems from PSI emission. The minor bands peaking around 650 and 660 nm can be attributed to PBS emission. In contrast to

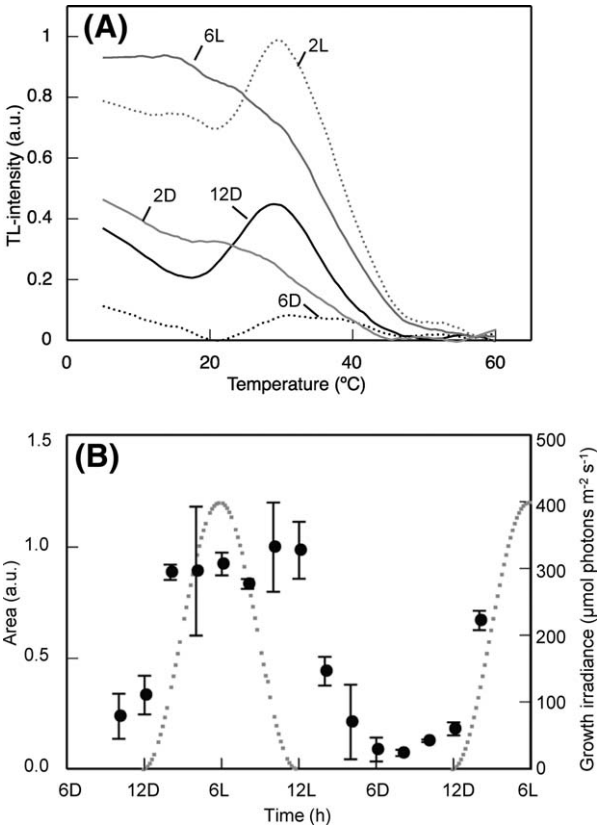

Fig. 4. Diel changes in the abundance of active PSII centres in *C. watsonii* as visualized by TL measurements. (A) Selected glow curves. Captions indicate the time (in hours) after the start of the corresponding light (L) or dark (D) period. (B) Areas under TL glow curves over the diel cycle. Averages of two independent measurements are shown with standard deviations as error bars.

daylight spectra, spectra collected during the dark phase (4D–8D) showed both the major F685 and F715, and the minor PBS bands. However, the fluorescence stemming from active PSII (F693) was largely reduced, indicating a substantial reduction of the photochemically active PSII during the dark phase. The substantial increase of F685, conversely, suggests exciton decoupling of PBS from the PSII reaction centres (Tamary *et al*., 2012, Barthel *et al*., 2013), which was particularly pronounced on PBS excitation (516 nm, Fig. 5B and C) as indicated by a more than $>$ 50% increase in F685 during the light-to dark transition (Supporting Information Fig. S1B). This finding is in good agreement with the observed increase in F_o during N_2 fixation phase (see Fig. 3 above and Discussion). Unlike the 77K spectra, the absorption spectra did not differ between the light and dark phase (Fig. 5C).

Diel change of PSI abundance and activity

Surprisingly, intracellular Chl also showed a dynamic diel pattern with maxima around at mid-day and minima in the

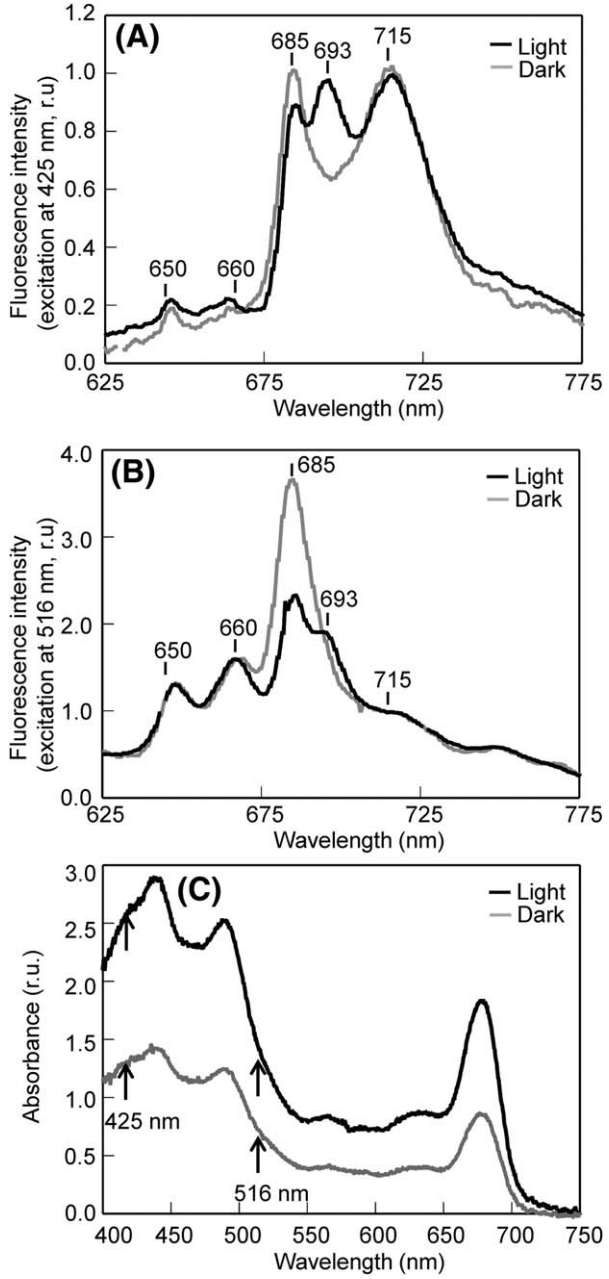

Fig. 5. 77K fluorescence emission- and absorption spectra of *C. watsonii* measured 4–8 h into the light period (4–8L) and 4–8 h into the dark (4–8D) phases. Fluorescence emission spectra were recorded on Chl (A, 425 nm) and PBS excitation (B, 515 nm), were averaged and normalized to the PSI peak/shoulder at 715 nm. (C) Absorption spectra of *C. watsonii* were shown as a reference with arrows indicating the excitation wavelengths.

middle of the night (Fig. 6A). Because most of the Chl in cyanobacteria is associated with PSI (Mullet *et al.*, 1980; Guskov *et al.*, 2009), the decline in Chl during the night could be attributed to a concomitant decrease in PSI abundance. We confirmed this notion by quantifying the content and the photochemical activity of PSI over the diel cycle using absorbance changes of the PSI primary electron donor P_{700}. During the first 6 h of the light period, the maximal P_{700} signal intensity (P_m'$_{max}$), which is proportional to the functional PSI content, increased by $\sim$ 30% just like Chl content. During the second half of the light period and the first half of the dark period, both P_m'$_{max}$ and Chl declined reaching a minimum around 2D–4D (Fig. 6A and B). P_m'$_{max}$ and Chl increase again during the late dark period. The ratio of P_m'$_{max}$:[Chl] was stable and relatively low during the light period but increases by $\sim$ 30% by the middle of the dark period (6D) (Supporting Information Fig. S1A). During the second half of this period (6D–12D), P_m'$_{max}$:[Chl] decreased again, returning nearly daylight levels. The night-time decrease in PSII abundance and activity was also visible from PSI quantum yields [$Y(I)$] and quantum yields of non-photochemical energy dissipation in PSI due to donor side limitation [Y(ND)] (Supporting Information Fig S1B).

The product of the initial slope of the rapid light curve of PSI mediated electron transport rates ($tg\alpha_{ETR(I)}$) and P_m'$_{max}$ gives a realistic representation of the potential ETR(I) and shows a dynamic diel pattern with a more than twofold increase of PSI mediated electron transport during the middle of the day compared to the night (Fig. 6B). However, $Y(I)$ decreased $\sim$20% from light in the dark period (Supporting Information Fig. S1B). Combining all these observations, our results indicate that, although PSI content dropped in parallel with Chl during the night, the residual PSI complexes remained fully active.

Diel changes in thylakoid membrane protein complexes

To correlate the observed diel changes in PSII and PSI activities with the cellular content and organization of these complexes, we analysed cellular membrane protein complexes using a combination of clear native- (CN) and sodium dodecyl sulfate (SDS) gel electrophoresis (CN/SDS-PAGE) and immunoblotting. The colour scan of the CN gel with separated samples of equal Chl concentrations was dominated by green pigment proteins belonging to PSI and showed constant levels of both PSI monomers and trimers throughout the whole diel cycle (Fig. 7A). However, when the gel was loaded on the same OD_{750} basis, significant fluctuations in PSI protein levels were observed which were in agreement with the diel changes in PSI and Chl content (data not shown).

Unlike the colour scan, Chl fluorescence images mostly reflect PSII-Chl-protein abundance. Thus, even when the gel was loaded on the same Chl basis, fluorescence scans clearly showed a pronounced decline in the abundance of PSII monomers and especially PSII dimers, which disappeared completely during the middle of the night (Fig. 7B). Concomitant to this disappearance of PSII core complexes, the fluorescence of small Chl-proteins belonging to

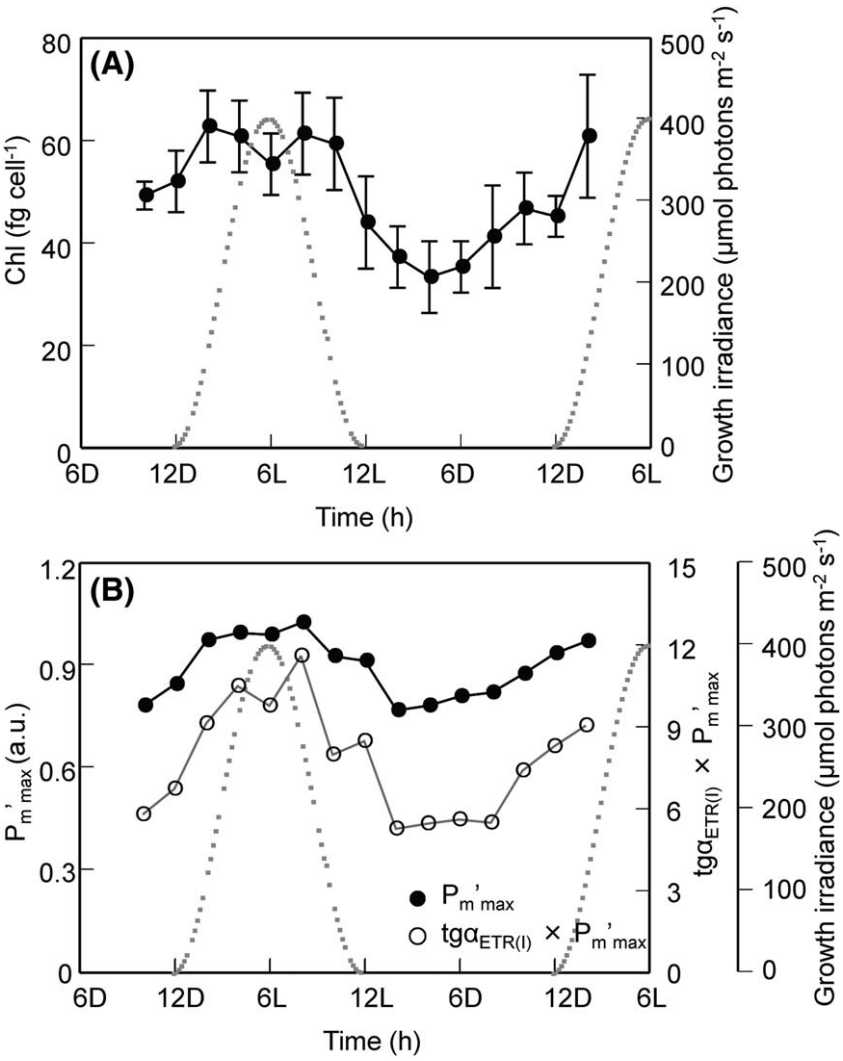

Fig. 6. Chl-concentration, PSI-abundance and activity in *C. watsonii*. (A) Diel pattern of Chl concentrations. $n = 3$, error bars are standard deviations. (B) Diel pattern of relative PSI content ($P_m'_{max}$) and PSI-mediated putative electron transport ($P_m'_{max} \times tg\alpha_{ETR(I)}$) as determined by PSI light response curves.

the free unassembled PSII core antenna proteins CP47 and CP43 gradually increased (Fig. 7). The immunoblot suggests the disappearance of large PSII core complexes due to the degradation of both of the PSII reaction centre proteins D1 and D2. To assess whether the disappearance of PSII complexes is related to the dark accumulation of FtsH proteases known to degrade the D1 and D2 subunits in cyanobacteria (Silva *et al*., 2003, Komenda *et al*., 2006, Nixon *et al*., 2010), we probed their cellular level with specific antibodies recognizing all FtsH forms. The results showed that 6D cells contained even lower levels of FtsH than those from 6L. In summary, these results confirmed that during the night, the abundance of PSII core complexes decreased more strongly than PSI complexes. This preferential disappearance of PSII core complexes and accompanying decrease in the level of D1 and D2 proteins was in agreement with TL data and 77K spectra and these were apparently not related to an excessive accumulation of FtsH proteases.

Decreased membrane protein synthesis is responsible for PSII depletion in the dark

We speculated that the observed decline in PSII activity and abundance in the dark could be a consequence of the light-induced modification of PSII complexes that triggers the degradation of the D1 protein while its replacement by a new functional copy cannot occur. To test this hypothesis, we radioactively labelled cells from 6L and 6D samples and analysed the labelled membrane proteins isolated from these cells by 2D CN/SDS-PAGE. While the strongly labelled bands of the D1 protein in the dimeric and monomeric PSII core complexes as well as in the core complex lacking CP43 (RC47) dominated the 2D autoradiogram of the 6L cells, 6D cells hardly showed any detectable levels of D1 biosynthesis (Supporting Information Fig. S2). At this time, radioactive labelling of the CP47, D2 and D1 subunits comprised only $19 \pm 2\%$, $25 \pm 2\%$ and $30 \pm 6\%$, respectively, of that at 6L, indicating a strong impairment of

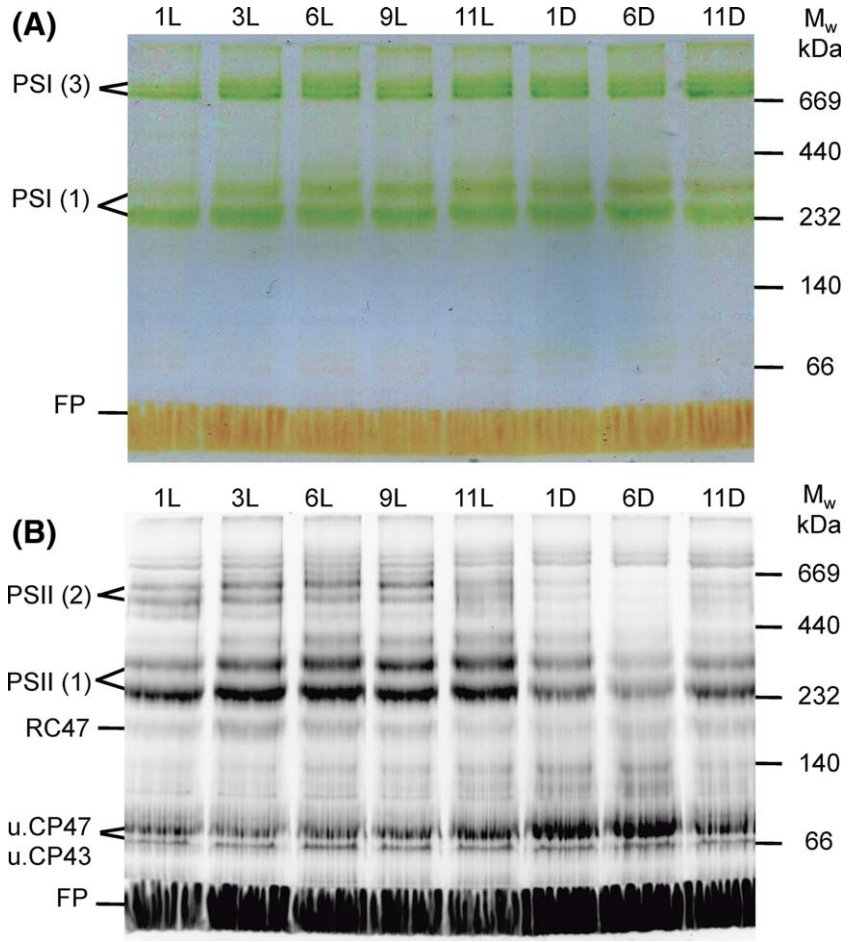

Fig. 7. Diel changes in abundance of membrane pigment-binding protein complexes in *C. watsonii* at 1L, 3L, 6L, 9L, 11L, 1D, 6D and 11D. Isolated membrane proteins were analysed by CN PAGE; the gel was photographed (A) and scanned to map Chl fluorescence with a camera system, ImageQuant LAS 4000 (B). Gel lanes 6L and 6D were used for 2D SDS PAGE and immunodetection of specific PSI and PSII subunits in Fig. 8. Each loaded sample contained 5 μg of Chl. Designation of complexes: PSI (3) and PSI (1), trimeric and monomeric PSI complexes respectively; PSII (2) and PSII (1), dimeric and monomeric core PSII complexes, respectively; RC47, PSII complex lacking CP43, u.CP43 and u.CP47, unassembled CP43 and CP47; F.P., free pigments.

the biosynthesis of the D1 and other core PSII subunits and explaining the drop in PSII activity and disassembly of PSII during the dark.

C. watsonii contains a specific *psbA* gene (designated *psbA4*) encoding the so-called rogue D1 (rD1) (Murray, 2012), however, the incorporation of rD1 into PSII has never been unequivocally shown. Using two specific antibodies recognizing the N-termini of rD1 and the standard functional D1 protein (fD1), respectively, we determined the abundance of both D1 forms and their distribution in various PSII complexes at 6L and 6D (Fig. 8). While fD1 was present in both dimeric and monomeric PSII core complexes at 6L, rD1 was absent in these cells. At 6D, PSII dimers containing fD1 disappeared and level of monomeric PSII complexes containing fD1 remained much lower than at 6L. Conversely, rD1 appeared at 6D and was assembled exclusively within monomeric PSII core complexes. A comparison of the blotted signals of CP47, D2 and fD1 in all PSII core complexes at 6L and 6D showed a 70%–80% decrease in the level of all of these three subunits at 6D relative to 6L. It showed that at 6D the actual level of the complexes containing rD1 is quite low, not exceeding 10% of the level of the PSII core complexes at 6L.

To elucidate whether the PSII inactivation and disassembly in the dark phase is related to the light exposure during the light phase, or whether it was a consequence of the diel cycle regulation, we manipulated the light conditions after the middle of the light phase (6L) of the diel cycle. In a first set of experiments, cells grown under a L:D cycle were kept at a maximal irradiance (400 μmol quanta m^{-2} s^{-1}) for the remaining 18 h of the light cycle on reaching the 6L time point. We followed changes in PSII activity and organization during this period by Chl fluorescence measurements and fluorescence scans of CN gels. Exposure to constant maximal irradiance resulted in a fast decline in F_v/F_m as compared to cells grown in the regular light/dark cycle (Fig. 9A; compare values from 6L to subjective 'midnight', s12D on day 2 and from 6L to 6D on day 1), a lack of recovery of PSII activity between s12D and s17D, and a drastic decrease in the abundance of PSII protein complexes. The latter was visualized by fluorescence scans of native gels which revealed a severe degradation and almost a complete loss of PSII core complexes by s12D (Fig. 9C).

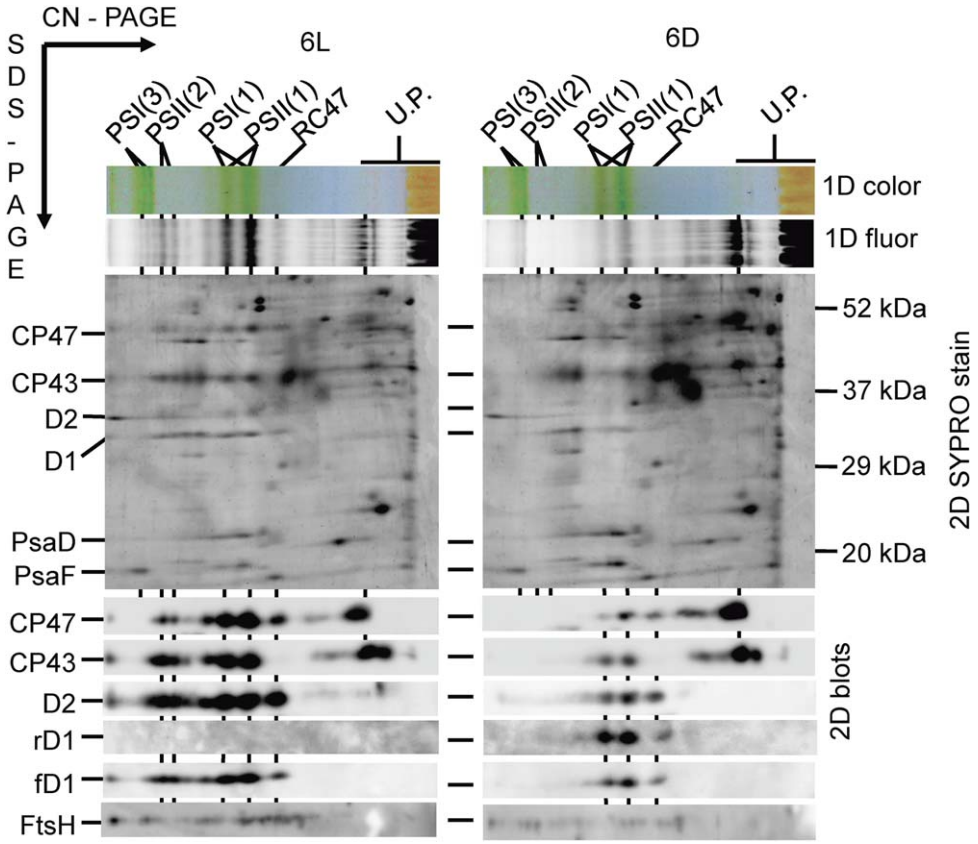

Fig. 8. Two-dimensional analysis of membrane protein complexes in *C. watsonii* cells 6 h into the light (L6) and 6 h into the dark (D6) phases. Membrane protein complexes were separated by CN PAGE (see also Fig. 7) and then subjected to an SDS-PAGE in the second dimension. The resulting gel was stained by SYPRO Orange (2D SYPRO stain), electroblotted to PVDF membrane and probed with antibodies (2D blots) specific for CP47, CP43, D2, rD1, fD1 and FtsH. Designation of complexes as in Fig. 7, U.P. are unassembled proteins.

Conversely, when illumination was switched off at the middle of the standard light cycle and the cells were kept in the dark from this point on, the decrease in PSII activity was much smaller as compared to the regular 12:12 cycle (Fig. 9B). This supports the notion that the observed loss of PSII is related to the light-induced PSII modification followed by the degradation of the D1 and D2 proteins together with the diel cycle.

Effect of N_2 fixation on PSII activity

To determine how nitrogenase activity influences diel changes in PSII organization and function, we inhibited N_2 fixation by adding 0.1 mM NH_4Cl to a diazotrophic culture at 6L. As compared to control cells growing exclusively under diazotrophic regime, addition of NH_4^+ remarkably slowed down the decline of the PSII activity during the subsequent dark phase. This implied a substantial residual PSII activity during the night (nocturnal minimum of F_v/F_m in the presence of NH_4^+ was about 0.12) while it was virtually zero in the diazotrophic control (Supporting Information Fig. S3A). Also, protein analysis showed higher PSII abundance during the dark phase in samples amended with NH_4^+ as compared to the control (compare Fig. 7 and Supporting Information Fig. S3B).

Discussion

In *C. watsonii*, N_2 fixation is restricted to the dark period, peaking during the second half of the night and then ending abruptly (Fig. 1). Photosynthetic capacity estimated by both O_2 evolution and ^{14}C assimilation, conversely, is maximal at mid-day but minimal at midnight, with O_2 evolving capacity decreasing virtually to zero while minimal C fixation rates were still about 20% of their maxima (Fig. 1). We speculate that the latter is probably due to a partial reactivation of C uptake initiated by the relatively long (30 min) exposure to actinic light during the ^{14}C incubation as compared to the short (3 min) exposure during the O_2 measurements. Diel patterns of the corresponding parameters in *Cyanothece* sp. were similar to those in *C. watsonii*; however, in *Cyanothece*, N_2 fixation reaches its maximum at the beginning of the dark period, and O_2 evolution during the night does not decrease below 40% of its daylight peaks (Colón-López and Sherman, 1998; Meunier *et al.*, 1997; 1998).

Diel changes of O_2 evolution, F_v/F_m, TL and 77K fluorescence emission spectra show that PSII in *C. watsonii* is fully active during the light period, and becomes inactivated during the dark (Figs 1, 2, 4 and 5). This is in good agreement with previous reports analysing fluorescence signals (Pennebaker *et al.*, 2010, Rabouille and Claquin, 2016), gene transcripts (Mohr *et al.*, 2010, Shi *et al.*, 2010) and

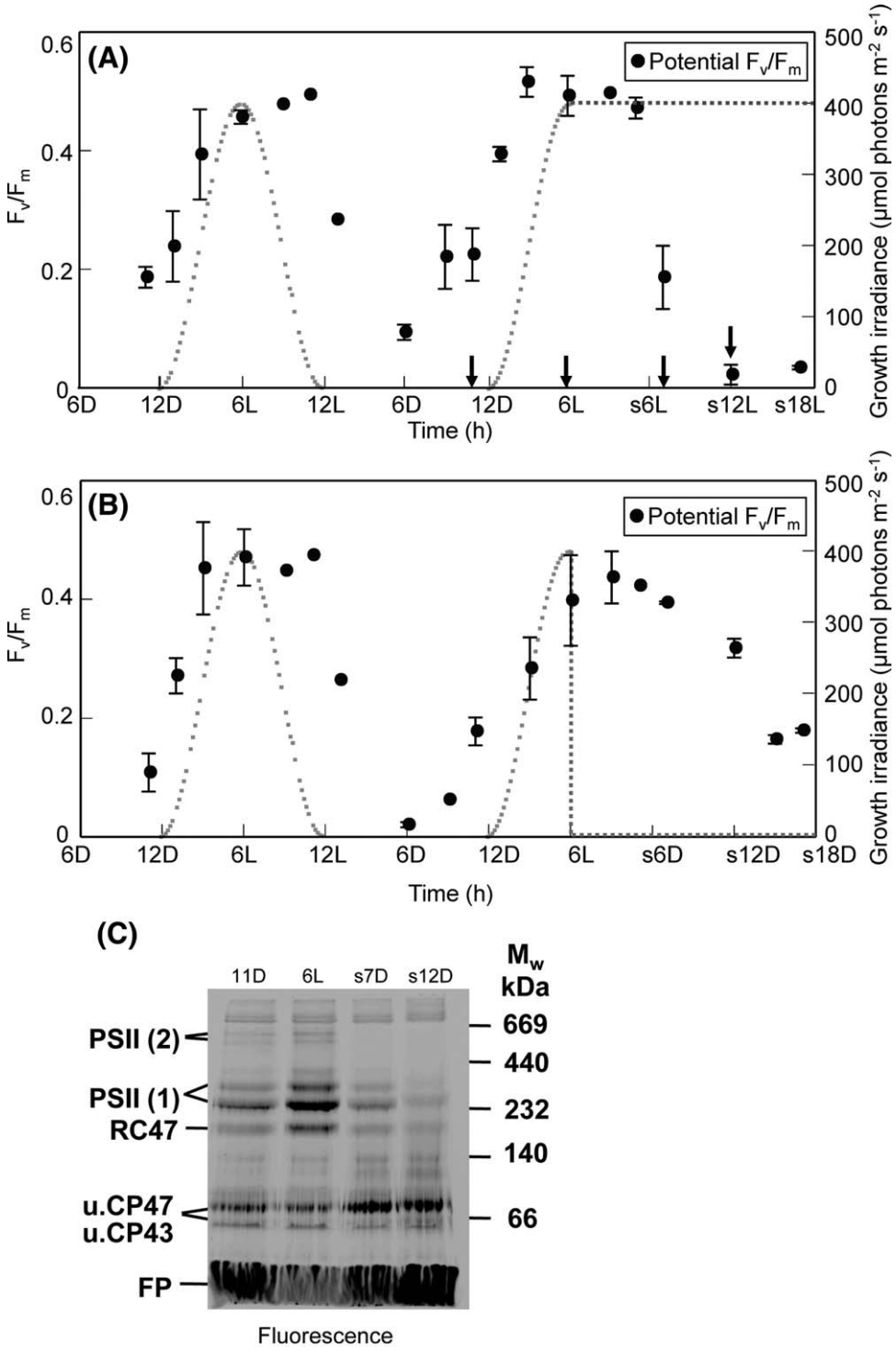

Fig. 9. Temporal changes in the potential F_v/F_m (see Fig. 2 and Experimental procedure) in *C. watsonii* transferred to 18 h of continuous light (A) and into darkness (B) after reaching 6L on day 2. Dotted lines indicate the pattern of the growth irradiance. Error bars indicated standard deviations ($n = 3$). (C) Fluorescence analysis of Chl-protein complexes in *C. watsonii* during the continuous light experiment presented in **A**. Samples were taken at 11D, 6L, s1D and s6D (arrows) phases of the diel cycle.

protein abundance (Mohr *et al.*, 2010, Saito *et al.*, 2011); all of which concluded that PSII activity during the day is considerably higher than during the night. Monitoring F_t, F_o and F_m inside the bioreactor showed that diel changes in F_v/F_m were determined both by changes in intrinsic Chl fluorescence and by the loss of variable fluorescence F_v. The drastic increase in F_t and F_o from 10L to 5D (Fig. 3A) is a consequence of extensive decoupling of PBS from the PSII reaction centres (Tamary *et al.*, 2012, Barthel *et al.*, 2013) (Fig. 5), and possibly also the accumulation of unassembled CP43 and CP47 due to PSII degradation (Figs 7 and 8). Simultaneous recording of OD_{735} and Chl fluorescence yields (Fig. 3B) allowed us to interpret the diel pattern of F_v/F_m shown in Figs 2 and 3 in the following

way: When growth irradiance supports growth and active photosynthesis (marked as photosynthesis and growth phase in Fig. 3), F_t is low and OD_{735} rises. Since OD_{735} contains information about biomass and cellular scattering properties, an increase in OD_{735} may point to enhanced growth and accumulation of carbon storage compounds. As the intensity of growth irradiance decreases and growth ceases, F_t, F_0 and F_m almost double and F_v gradually disappears within a few hours while OD_{735} decreases only slightly (preparation for N_2 fixation phase in Fig. 3). This is the transition period when metabolism changes from photosynthesis to N_2 fixation, which begins at the end of the light period when the light irradiances drop roughly below 50 μmol quanta m^{-2} s^{-1}. This may reflect induction transition from State 2 to State 1 by a partial oxidation of the intersystem electron transfer chain and relaxation of non-photochemical quenching (NPQ) during peak irradiances by orange carotenoid protein (OCP) (Kirilovsky and Kerfeld, 2013). Both of these are required for maintaining photosynthetic activities under limited light conditions (Figs 1–5). Nitrogen fixation is detectable in the N_2 fixation phase starting at 3D when both, OD_{735} and F_o decrease in parallel and F_v drops to virtually zero. We interpret this phase as a decline in cellular Chl content (Figs 3 and 6) and the consumption of carbon storage compounds due to respiration that provides ATP for N_2 fixation. Eventually, at the end of the diel cycle (preparation for photosynthesis phase), OD_{735} remains constant while F_t rapidly decreases as active PSII complexes are re-assembled and photosynthetic (inner and outer) antennae are re-coupled to the photosystems again (Fig. 3). During preparation for photosynthesis phase, cells started to express variable fluorescence again, indicating a re-activation of photosynthetic electron transport and O_2 evolution as well as a concurrent transition from State 1 to State 2 and induction of OCP quenching as growth irradiance increases to $>$50 μmol photons m^{-2} s^{-1}. The difference in OD_{735} between first and second phases of preparation for photosynthesis represents the net growth of the culture over a diel cycle.

Protein analysis and immunodetection clearly showed that the loss of PSII activity was accompanied by the disappearance of both the monomeric and dimeric PSII core complexes as well as by a degradation of D1 and D2 subunits in the dark. The low abundance of FtsH proteases, which are involved in PSII protein degradation and their quality control (Silva *et al*., 2003, Komenda *et al*., 2006, Nixon *et al*., 2010), excludes the possibility that the observed decline in PSII abundance in the dark is related to enhanced proteolytic activity of overaccumulated FtsH proteases. Instead, our 2D autoradiograms showed that protein synthesis of D1 polypeptides was severely impaired during the dark period. In line with this, transcript analysis also revealed that the expression of *psbA* gene encoding functional D1 (fD1) proteins is strongly suppressed in the dark (Shi *et al*., 2010). Altogether, these results suggest that PSII reaction centre subunits during the dark phase were (i) severely degraded and (ii) not sufficiently re-synthesised. We believe that the impaired synthesis of membrane proteins, especially the functional D1 protein, may represent a protective mechanism that helps retain cellular resources for N_2 fixation during the dark phase. Interestingly, PSI as well as PSII core complexes were always separated into two bands but reason for this remains unknown. The two bands may reflect different conformation states of the complexes or different detergent/lipid binding to them.

Western blot analysis using specific antibodies unequivocally revealed the accumulation of an unusual, so-called rogue D1 form (Murray, 2012) in the monomeric PSII core complexes during the dark phase. Murray, (2012) reported rD1 is a non-functional version due to the absence of key amino acid residues essential for binding the oxygen evolving $CaMn_4O_5$ clusters. Wegener and colleagues (2014) also suggested that in *Cyanothece* this protein is incorporated into PSII complexes to eliminate their ability to evolve oxygen. Taking into account a large-scale disassembly of PSII and the overall decrease in intracellular Chl during this phase, the abundance of PSII complexes containing rD1 was negligible as compared to the level of functional PSII complexes during the light phase. In view of these results, the possible function of PSII complexes with rD1 remains unclear. In the dark, even functional PSII complexes cannot evolve O_2, hence, the previously suggested function of these complexes in preventing evolution of O_2 toxic for nitrogenase (Fay, 1992, Gallon and Stal, 1992) seems unlikely. Moreover, the abundance of PSII complexes containing functional D1 exceeds that of the rD1-containing complexes in the dark period. Considering the recently proposed role of another divergent D1 form in the synthesis of Chl *f* (Ho *et al*., 2016), an unknown enzymatic function of PSII complexes containing rD1 (e.g., dark cellular metabolism) cannot be excluded.

When the 12:12 light-dark cycle of the cells was modified by extending the light period, PSII disassembly and the decline in PSII activity during which the cells are exposed to the subjective light phase was enhanced (Fig. 9A). A shortening of the light period, conversely, resulted in a much slower decline in PSII activity during the subsequent dark phase (Fig. 9B and C). Similar phenomena were also observed by Pennebaker *et al*. (2010) who analysed photosynthetic activity under similar conditions with a maximum irradiance of only 100 μmol photons m^{-2} s^{-1}. They also reported a disruption of regular changes in photosynthetic efficiency during the diel cycle when cultures were shifted into an early dark phase, but not when they were shifted into continuous light. Combining our results with previous observation leads us to conclude that photoperiod length paces the temporal orchestration of the cell cycle

and of carbon-nitrogen metabolism (Dron *et al.*, 2013). We conclude that light history of the cells (length of photoperiod, light intensity) significantly affects the circadian rhythm of the photosynthetic activity in *C. watsonii*.

We also showed that relative changes in PSII activity and abundance were reduced by the availability of NH_4^+. After its addition, the nocturnal decline of F_v/F_m slowed down and the abundance of PSII complexes remained constant during the dark phase (Supporting Information Fig. S3), which is in good agreement with previous reports (Dixon and Kahn, 2004); however, the underlying mechanisms of this regulation are still to be elucidated. Possibly, NH_4^+ induces changes in the expression of some genes that are, directly or indirectly, related to N_2 fixation including genes required for down-regulating of PSII activity. Direct NH_4^+ effect to photosystems should be also considered in future study.

The decline in PSI abundance during the dark period as indicated by a decrease in cellular Chl and $P_m'_{max}$ as well as by CN PAGE normalized to Chl (Figs 6a, b and 7) is in agreement with mass spectrometer data showing a ~ 50% decline in the level of both PSI reaction centre subunits, PsaA and PsaB during the dark in *C. watsonii* (Saito *et al.*, 2011). However, other diazotrophic bacteria, like *Cyanothece* sp. showed a different behaviour, that is, a higher capacity for PSI-mediated electron transport in the dark period relative to the light phase (Colón-López and Sherman, 1998). Again, the reason for this and other differences between *Cyanothece* sp. and *C. watsonii* (see above) remains unclear. Furthermore, functional nitrogenase enzymes contain a high quantity of iron cofactors (in total 38 Fe atoms per nitrogenase complex) (Rubio and Ludden, 2008), and thus it has been argued that iron is supplied by the degradation of iron-rich PSI complexes (36 Fe per monomeric PSI) in *C. watsonii* (Saito *et al.*, 2011), similarly like shown in *Trichodesmium* IMS101 (Shi *et al.*, 2007). Such iron recycling is well documented in cyanobacteria like *Synechococcus elongatus* PCC7942 where photosynthetic protein complexes are degraded in the order of PSII, PSI, and cytochrome b_6f under iron deficiency, which prolongs survival by maintaining electron transport and energy transduction under iron stress (Pietsch *et al.*, 2011). Thus, the diel cycle of PSI in *C. watsonii* could be evolutionarily related to iron limitation in its natural habitat.

The degradation of PSI is rather interesting from the point of view of general quality control of photosynthetic membrane proteins as a high turnover rate is generally considered as a typical feature of PSII. The observed rapid changes in PSI abundance in cyanobacteria is very unusual and, thus far, has only been reported during iron stress (Bibby *et al.*, 2001). Also, decreased PSI abundance and a small, inactive PSII population is reported in *Synechocyctis* PCC 6803 grown under light activated heterotrophic growth conditions (Barthel *et al.*, 2013). However, under such conditions, an active degradation of PSI has never been proven and is most likely related to its dilution during cellular growth and division when PSI biosynthesis is blocked. In contrast to these findings, the rapid PSI decline in *C. watsonii* should be driven by a protease; however, thus far there is no experimental data for the existence of such cyanobacterial protease(s) being involved in the degradation of PSI. The FtsH proteases involved in the degradation of PSII subunits do not seem to be potential candidates as their cellular level is lower during the dark as compared to light phase. Nonetheless, the molecular nature of PSI degradation and accompanying Chl catabolism is still to be elucidated. In summary, the diel cycle of *C. watsonii* provides an interesting model system for studying cyanobacterial regulatory mechanisms, survival strategies and efficient utilization and recycling of cellular resources.

Experimental procedures

Strain, cultivation, experimental conditions and monitoring of growth

Stock cultures of *Crocosphaera watsonii* WH8501 obtained from The Culture Collection Yerseke (The Royal Netherlands Institute for Sea Research, Yerseke, The Netherlands strain number CCY 0601) were maintained in N-free YBC-II medium (Chen *et al.*, 1996) at 28°C in glass flasks under constant white light of 150 μmol quanta m^{-2} s^{-1} using a 12:12 h light:dark (12L:12D) cycle. Diluting them every ~ 12 days kept cell densities within 200 000 to 6 000 000 cells ml^{-1}. At the beginning of each experiment ($n = 9$), cultures were transferred into flat panel photobioreactors (FMT150, Photon System Instruments, Brno, Czech Republic) (Nedbal *et al.*, 2008) with a sinusoidal 12L:12D growth irradiance peaking at 400 μmol photons m^{-2} s^{-1}. Cultures were acclimated to these conditions and maintained in exponential growth for at least 5 generations (~ 10 days). The photobioreactors continuously recorded F_o and F_t (every 5 min) as well as F_m and F_m' (every 30 min), which were then used to calculate *in situ* diurnal changes in F_t and F_m by averaging data sets of 7 consecutive days. Biomass, diel change of F_t and F_0 data were normalized to the respective values measured every day 1 h after the light onset (1L), F_m values were re-calculated based on the normalized F_0 and F_t values and F_v/F_m data. Cell abundance was measured by a Coulter Counter (Beckman, Multisizer 4, Indianapolis, IN). To determine Chl *a* concentration, we collected 10 ml of culture on Whatman GF/F glass fibre filters and measured Chl *a* in pure methanol extracts by spectroscopy (Porra *et al.*, 1989).

To determine whether N_2 fixation affects diel changes of PSII activity, we added 100 μM NH_4Cl (final conc.) to a diazotrophically grown culture in the middle of a light period and then followed the changes in fluorescence as well as the abundance of PSII core complexes and unbound subunits for another complete L/D period.

Determination of N_2 fixation, O_2 evolution and C fixation rates

To determine the rates of N_2 fixation by acetylene reduction assays (Capone and Montoya, 2001), 5 ml of cell suspensions

were dispensed into HCl-rinsed glass vials ($n = 3$). After sealing each vial with a septum, 10 ml of acetylene gas (99.7% [v/v]; Linde Gas) was injected by replacing the same volume of headspace. The samples were incubated at 28°C in the dark for 1 h. Subsamples of the headspace were taken immediately after acetylene addition and then at the end of the incubation to measure their ethylene content with a flame ionization gas chromatograph (HRGC 5300, Carlo Erba Instruments). Ethylene production during the incubation was analysed, and produced ethylene was calculated according to Breitbarth (Breitbarth *et al.*, 2004) and converted to fixed N_2 using a theoretical molar ratio of acetylene reduction to cellular N_2 reduction of 4:1 (Montoya *et al.*, 1996).

O_2 evolution rates in the presence of 5 mM sodium bicarbonate were determined using a Clark electrode combined with a DW2/2 electrode chamber (Hansatech, UK) maintained at 28°C. Depending on the cell density, different culture volumes were concentrated by 10 min of centrifugation at 7500 *g* and re-suspended in 2.7 ml fresh YBC-II medium. Rate of gross O_2 evolution were calculated from the slope of net O_2 evolution measured at a saturating irradiance of 600 μmol photons m^{-2} s^{-1} (KL1500, Schott, Mainz, Germany) corrected for the slope of respiratory O_2 consumption measured in the dark right after the light exposure.

Carbon fixation rates were determined by short-term incubations with radioactively labelled $NaH^{14}CO_3$ using a photosynthetron (Lewis and Smith, 1983). Briefly, 5 ml of culture were mixed with 31 ml of YBC-II medium, which were then supplemented with $NaH^{14}CO_3$ (ARC American Radiolabeled Chemicals, St. Louis, MO) (final concentration 1 μCi ml^{-1}) and incubated for 30 min at 28°C at light intensities at a saturating irradiance of 600 μmol photons m^{-2} s^{-1}. After incubation, samples were immediately preserved with buffered formalin, acidified with 3N HCl (final concentration 0.75 mol l^{-1}) and left to degas on an orbital shaker for at least 5 h. Aliquots of 5 ml of EcoLite™ liquid scintillation cocktail (MP Biomedicals, LLC, Solon, OH) were added to each of the vials, which were then capped and their activity counted in a TriCarb 2810TR Perkin Elmer Liquid Scintillation Analyzer. Counts per minute were converted to carbon fixation rates according to Knap *et al.* (Knap *et al.*, 1996). Chl-specific carbon fixation rates were plotted against irradiance to derive the maximum carbon fixation rates (P_{max}, mg C (mg Chl)$^{-1}$ h^{-1}) by fitting the model of Eilers and Peeters (Eilers and Peeters, 1988) to the measured data. Finally, Chl-specific carbon fixation rates were converted to cell-specific carbon fixation rates using the corresponding cell densities and Chl *a* concentrations.

Determination of Chl fluorescence parameters

Fluorescence yields were determined in two separate ways: (i) by recording F_o, F_t and F_m *in situ* in the bioreactor as mentioned above and (ii) by measuring F_v ($= F_m - F_o$) and F_m in 2 ml aliquots withdrawn from the bioreactor using a portable AquaPen-C AP-C100 fluorometer (Photon Systems Instruments, Brno, Czech Republic). To avoid the influence of state transitions on these fluorescence yields (see Fig. 3 and corresponding text in Results and Discussion), we determined F_v/F_m after exposing each sample for 5 min to a weak (30 μmol photons m^{-2} s^{-1}) blue (445 nm) light which oxidises all components of the intersystem electron transport chain, and thus, induced State 1.

Thermoluminescence glow curves

TL glow curves were recorded using a TL 200/PMT thermoluminescence (TL) system (Photon Systems Instruments, Brno, Czech Republic) on 3 ml of cell suspension, which were filtered onto a Pragopor 5 nitrocellulose membrane filter (pore size 0.6 ± 0.1 μm; Pragopor, Czech Republic) and placed on the instrument's sample holder. After 2 min of dark acclimation at 28°C, samples were cooled down to 3°C and exposed to two subsequent saturating single turnover flashes (50 μs, 200 ms apart) followed by the heating/recording phase. TL curves were recorded from 3°C to 65°C with a linear heating rate of 0.5°C s^{-1}. The amount of active PSII centres was then determined by integrating the area under each glow curves.

Photosystem I activity

Photosystem I activity was estimated using a Dual-PAM-100 system (Walz GmbH, Effeltrich, Germany) on 10 mL of culture filtered onto a Pragopor 5 nitrocellulose membrane filter (as above). Filters were placed between the perspex rods of the emitter (DUAL-E) and the detector (DUAL-DR) using a DUAL-B leaf clip holder. P_{700} light response curves were recorded using actinic red light with light intensity increasing in 10 logarithmic increments from 0 to 1950 μmol photons m^{-2} s^{-1} with each light level being applied for 120 s. At the end of each step, saturating pulses of 30 ms duration and 10.000 μmol photons m^{-2} s^{-1} intensity were applied to probe maximal P_{700} levels in actinic light (P_m'). Quantum yields of photochemical energy conversion of PSI [$Y(I)$], quantum yields of non-photochemical energy dissipation in PSI due to donor side limitation [Y(ND)], and PSI mediated apparent electron transport rates [ETR(I)] were determined using the DualPAM software (V1.19) provided by Walz company. Maximal P_m values ($P_{m'max}$) over the light response curves were used to visualize the abundance of active PSI centres.

Low temperature fluorescence spectra and absorption spectra

Fluorescence emission spectra were recorded at 77K using an SM-9000 spectrofluorometer (Photon Systems Instruments, Brno, Czech Republic) every 2 h. Cells were dark acclimated at room temperature for 10 min and then collected on Whatman GF/F glass fibre filters, which were cut and placed into a custom-made copper sample holder and then immersed into a glass Dewar filled with liquid N_2. Fluorescence was excited at 425 and at 516 nm (Scheer, 2003; Papageoriou, 2004) and recorded with 500 ms of integration time and an amplification of 800 from 620 to 820 nm ($n = 3$). Spectra were baseline-corrected using a blank sample and normalized to the peak/shoulder at 715 nm. Absorption spectra were measured with a Unicam UV/vis 500 spectrometer equipped with an integrating sphere (Thermo Spectronic, UK) on samples collected on membrane filters (pore size 0.6 μm; Pragochema, Czech Republic).

Radioactive labelling of proteins

For radioactive protein labelling, cells were harvested at the middle of the light (6L) and dark (6D) period, resuspended in 250 μl YBC-II medium and incubated either at 400 μmol photons m^{-2} s^{-1} (6L sample) or in darkness (6D sample). Then, L-[^{35}S]-methionine (Hartmann Analytics, Braunschweig, Germany; specific activity > 37 TBq/mmol) was added (final specific activity 400 μCi ml^{-1}) to each suspension, which was then incubated under aforementioned conditions for another 30 min. On completion of the incubation, cells were frozen in liquid N_2 and stored at −80°C until thylakoid membrane protein isolation (see below).

Preparation of membranes and protein analyses

Cyanobacterial membrane proteins were isolated by breaking cells with glass beads and membranes in 1% n-dodecyl-β-D-maltoside to analyse their proteins by clear native (CN) PAGE (Komenda *et al.*, 2012). Samples of equal Chl content (5 μg) were loaded onto the gel. The protein composition of the complexes was analysed by electrophoresis in a denaturing 12%–20% linear gradient polyacrylamide gel containing 7 M urea. Gels with separated proteins were stained with either Coomassie Blue or SYPRO Orange and then transferred onto a polyvinylidene difluoride (PVDF) membrane. PVDF membranes were incubated with specific primary antibodies against D1, D2, CP47 and CP43 subunits and against FtsH recognizing all FtsH forms present in cyanobacteria (Boehm *et al.*, 2012), then with secondary antibody-horseradish peroxidase conjugate (Sigma, St. Louis, MO). Antibody specific for rD1 was raised in rabbit against a conjugate of keyhole limpet hemocyanin with a peptide 2-15 of rD1 and purified using the immobilized peptide. For autoradiography, the membrane with labelled proteins was exposed to a Phosphorimager plate (GE Healthcare, Uppsala, Sweden) overnight and the abundance of CP47, D2, fD1 and rD1 polypeptides on the stained 2D gels was quantified using ImageQuant LAS 4000 (GE Healthcare, Uppsala, Sweden) software.

Acknowledgements

We would like to thank Gabor Steinbach for providing us with a software package for analysing the bioreactor data. This research was supported by Grant Agency of the Czech Republic GACR (project 16–15467S) and the Ministry of Education of the Czech Republic, (projects LO1416 and CZ 1.05/2.1.00/19.0392).

References

Andrizhiyevskaya, E.G., Chojnicka, A., Bautista, J.A., Diner, B.A., van Grondelle, R., and Dekker, J.P. (2005) Origin of the F685 and F695 fluorescence in Photosystem II. *Photosyn Res* **84:** 173–180.

Barthel, S., Bernát, G., Seidel, T., Rupprecht, E., Kahmann, U., and Schneider, D. (2013) Thylakoid membrane maturation and PSII activation are linked in greening *Synechocystis* sp. PCC 6803 cells. *Plant Physiol* **163:** 1037–1046.

Berman-Frank, I., Lundgren, P., Chen, Y.B., Küpper, H., Kolber, Z., Bergman, B., *et al.*, (2001) Segregation of nitrogen fixation and oxygenic photosynthesis in the marine cyanobacterium Trichodesmium. *Science* **294:** 1534–1537.

Berman-Frank, I., Lundgren, P., and Falkowski, P. (2003) Nitrogen fixation and photosynthetic oxygen evolution in cyanobacteria. *Res Microbiol* **19:** 162–173.

Bibby, T.S., Nield, J., and Barber, J. (2001) Iron deficiency induces the formation of an antenna ring around trimeric photosystem I in cyanobacteria. *Nature* **412:** 743–745.

Boehm, M., Yu, J., Krynicka, V., Barker, M., Tichy, M., Komenda, J., Nixon, P.J., and Nield, J. (2012) Subunit organization of a synechocystis hetero-oligomeric thylakoid FtsH complex involved in photosystem II repair. *Plant Cell* **24:** 3669–3683.

Breitbarth, E., Mills, M.M., Friedrichs, G., and LaRoche, J. (2004) The Bunsen gas solubility coefficient of ethylene as a function of temperature and salinity and its importance for nitrogen fixation assays. *Limnol Oceanogr Meth* **2:** 282–288.

Capone, D.G., and Montoya, J.P. (2001) Nitrogen fixation and denitrification. *Method Microbiol* **30:** 501–515.

Chen, Y.B., Zehr, J.P., and Mellon, M. (1996) Growth and nitrogen fixation of the diazotrophic filamentous nonheterocystous cyanobacterium *Trichodesmium* sp IMS 101 in defined media: evidence for a circadian rhythm. *J Phycol* **32:** 916–923.

Church, M.J., Short, C.M., Jenkins, B.D., Karl, D.K., and Zehr, J.P. (2005) Temporal patterns of nitrogenase gene (*nifH*) expression in the oligotrophic North Pacific Ocean. *Appl Environ Microbiol* **71:** 5362–5370.

Colón-López, M.S., and Sherman, L.A. (1998) Transcriptional and translational regulation of photosystem I and II genes in light-dark- and continuous-light-grown cultures of the unicellular cyanobacterium *Cyanothece* sp. strain ATCC 51142. *J Bacteriol* **180:** 519–526.

D'Haene, S.E., Sobotka, R., Bucinska, L., Dekker, J.P., and Komenda, J. (2015) Interaction of the PsbH subunit with a chlorophyll bound to histidine 114 of CP47 is responsible for the red 77 K fluorescence of Photosystem II. *BBA-Bioenergetics* **1847:** 1327–1334.

Demeter, S., and Vass, I. (1984) Charge accumulation and recombination in Photosystem-II studied by thermoluminescence. 1. Participation of the primary acceptor-Q and secondary acceptor-B in the generation of thermoluminescence of chloroplasts. *BBA-Bioenergetics* **764:** 24–32.

Dixon, R., and Kahn, D. (2004) Genetic regulation of biological nitrogen fixation. *Nat Rev Microbiol* **2:** 621–631.

Dron, A., Rabouille, S., Claquin, P., Le Roy, B., Talec, A., and Sciandra, A. (2012) Light-dark (12:12) cycle of carbon and nitrogen metabolism in *Crocosphaera watsonii* WH8501: relation to the cell cycle. *Environ Microbiol* **14:** 967–981.

Dron, A., Rabouille, S., Claquin, P., Talec, A., Raimbault, V., and Sciandra, A. (2013) Photoperiod length paces the temporal orchestration of cell cycle and carbon-nitrogen metabolism in *Crocosphaera watsonii*. *Environ Microbiol* **15:** 3292–3304.

Dugdale, R.C., Menzel, D.W., and Ryther, J.H. (1961) Nitrogen fixation in the Sargassi Sea. *Deep-Sea Res* **7:** 298–300.

Eilers, P.H.C., and Peeters, J.C.H. (1988) A Model for the relationship between light-intensity and the rate of photosynthesis in phytoplankton. *Ecol Model* **42:** 199–215.

Fay, P. (1992) Oxygen relations of nitrogen-fixation in cyanobacteria. *Microbiol Rev* **56:** 340–373.

Gallon, J.R., and Stal, L.J. (1992) N_2 fixation in nonheterocystous cyanobacteria - an overview. In *Marine Pelagic Cyanobacteria: Trichodesmium and Other Diazotrophs*. Carpenter E.J., Capone D.G., Rueter J.G. (eds). The Netherlands: Kluwer Academic Publishers, pp. 115–139.

Guskov, A., Kern, J., Gabdulkhakov, A., Broser, M., Zouni, A., and Saenger, W. (2009) Cyanobacterial photosystem II at 2.9Å resolution and the role of quinones, lipids, channels and chloride. *Nat Struct Mol Biol* **16:** 334–342.

Ho, M.Y., Shen, G.Z., Canniffe, D.P., Zhao, C., and Bryant, D.A. (2016) Light-dependent chlorophyll f synthase is a highly divergent paralog of PsbA of photosystem II. *Science* **353:** aaf9178. 10.1126/science.aaf9178.

Karl, D., Letelier, R., Tupas, L., Dore, J., Christian, J., and Hebel, D. (1997) The role of nitrogen fixation in biogeochemical cycling in the subtropical North Pacific Ocean. *Nature* **388:** 533–538.

Kirilovsky, D., and Kerfeld, C.A. (2013) The orange carotenoid protein: a blue-green light photoactive protein. *Photochem Photobiol Sci* **12:** 1135–1143.

Kirilovsky, D., Kaňa, R., and Prášil, O. (2015) Mechanisms modulating energy arriving at reaction centers in cyanobacteria. In *Non-Photochemical Quenching and Energy Dissipation in Plants, Algae and Cyanobacteria*. Dordrecht: Springer Science + Business, pp 471–501.

Knap, A.H., Michaels, A., Close, A.R., Ducklow, H., and Dickson, A.G. (1996) *Protocols for the Joint Global Ocean Flux Study (JGOFS) Core Measurements*, JGOFS Report Number 19. Paris: UNESCO, p. 179.

Komenda, J., Barker, M., Kuvikova, S., de Vries, R., Mullineaux, C.W., Tichy, M., and Nixon, P.J. (2006) The FtsH protease slr0228 is important for quality control of photosystem II in the thylakoid membrane of *Synechocystis* sp PCC 6803. *J Biol Chem* **281:** 1145–1151.

Komenda, J., Knoppova, J., Kopecna, J., Sobotka, R., Halada, P., Yu, J.F., *et al.* (2012) The Psb27 assembly factor binds to the CP43 complex of photosystem II in the cyanobacterium *Synechocystis* sp PCC 6803. *Plant Physiol* **158:** 476–486.

Lee, K., Karl, D.M., Wanninkhof, R., and Zhang, J.Z. (2002) Global estimates of net carbon production in the nitrate-depleted tropical and subtropical oceans. *Geophys Res Lett* **29:** 13-1. doi:10.1029/2001GL014198.

Lewis, M.R., and Smith, J.C. (1983) A small volume, short-incubation-time method for measurement of photosynthesis as a function of incident irradiance. *Mar Ecol Prog Ser* **13:** 99–102.

Meunier, P.C., Colon-Lopez, M.S., and Sherman, L.A. (1997) Temporal changes in state transitions and photosystem organization in the unicellular, diazotrophic cyanobacterium *Cyanothece* sp. ATCC 51142. *Plant Physiol* **115:** 991–1000.

Meunier, P.C., Colón-López, M.S., and Sherman, L.A. (1998) Photosystem II cyclic heterogeneity and photoactivation in the diazotrophic, unicellular cyanobacterium *Cyanothece* species ATCC 51142. *Plant Physiol* **116:** 1551–1562.

Mohr, W., Intermaggio, M.P., and LaRoche, J. (2010) Diel rhythm of nitrogen and carbon metabolism in the unicellular, diazotrophic cyanobacterium *Crocosphaera watsonii* WH8501. *Environ Microbiol* **12:** 412–421.

Moisander, P.H., Beinart, R.A., Hewson, I., White, A.E., Johnson, K.S., Carlson, C.A., Montoya, P., and Zehr, J.P. (2010) Unicellular cyanobacterial distributions broaden the oceanic N_2 fixation domain. *Science* **327:** 1512–1514.

Montoya, J.P., Voss, M., Kahler, P., and Capone, D.C. (1996) A simple, high-precision, high sensitivity tracer assay for N_2 fixation. *Appl Environ Microbiol* **62:** 986–993.

Montoya, J.P., Holl, C.M., Zehr, J.P., Hansen, A., Villareal, T.A., and Capone, D.G. (2004) High rates of N_2 fixation by unicellular diazotrophs in the oligotrophic Pacific Ocean. *Nature* **430:** 1027–1031.

Mullet, J.E., Burke, J.J., and Arntzen, C.J. (1980) Chlorophyll proteins of photosystem I. *Plant Physiol* **65:** 814–822.

Murray, J.W. (2012) Sequence variation at the oxygen-evolving centre of photosystem II: a new class of 'rogue' cyanobacterial D1 proteins. *Photosyn Res* **110:** 177–184.

Nedbal, L., Trtilek, M., Cerveny, J., Komarek, O., and Pakrasi, H.B. (2008) A photobioreactor system for precision cultivation of photoautotrophic microorganisms and for high-content analysis of suspension dynamics. *Biotechnol Bioeng* **100:** 902–910.

Nixon, P.J., Michoux, F., Yu, J., Boehm, M., and Komenda, J. (2010) Recent advances in understanding the assembly and repair of photosystem II. *Ann Bot* **106:** 1–16.

Papageoriou, G.C. (2004) Fluorescence of photosynthetic pigments in vitro and in vivo. In *Advances in Photosynthesis and Respiration, Vol.19, Chlorophyll Fluorescence: A Signature of Photosynthesis*. Papageorgiou, G. C., Govindjee (eds). Berlin: Springer, pp. 43–63.

Pennebaker, K., Mackey, K.R.M., Smith, R.M., Williams, S.B., and Zehr, J.P. (2010) Diel cycling of DNA staining and nifH gene regulation in the unicellular cyanobacterium *Crocosphaera watsonii* strain WH 8501 (Cyanophyta). *Environ Microbiol* **12:** 1001–1010.

Pietsch, D., Bernát, G., Kahmann, U., Staiger, D., Pistorius, E.K., and Michel, K.P. (2011) New insights into the function of the iron deficiency-induced protein C from *Synechococcus elongatus* PCC 7942. *Photosyn Res* **108:** 121–132.

Porra, R.J., Thompson, W.A., and Kriedemann, P.E. (1989) Determination of accurate extinction coefficients and simultaneous-equations for assaying chlorophylls *a* and *b* extracted with four different solvents: verification of the concentration of chlorophyll standards by atomic-absorption spectroscopy. *BBA-Bioenergetics* **975:** 384–394.

Rabouille, S., and Claquin, P. (2016) Photosystem-II shutdown evolved with nitrogen fixation in the unicellular diazotroph *Crocosphaera watsonii*. *Environ Microbiol* **18:** 477–485.

Rubio, L.M., and Ludden, P.W. (2008) Biosynthesis of the iron-molybdenum cofactor of nitrogenase. *Annu Rev Microbiol* **62:** 93–111.

Rutherford, A.W., Crofts, A.R., and Inoue, Y. (1982) Thermoluminescence as a probe of Photosystem II photochemistry. The origin of the flash-induced glow peaks. *BBA Bioenergetics* **682:** 457–465.

Saito, M.A., Bertrand, E.M., Dutkiewicz, S., Bulygin, V.V., Moran, D.M., Monteiro, F.M., *et al.* (2011) Iron conservation by reduction of metalloenzyme inventories in the marine diazotroph *Crocosphaera watsonii*. *Proc Natl Acad Sci USA* **108:** 2184–2189.

Scheer, H. (2003) The pigments. In *Advances in Photosynthesis and Respiration Vol 13, Light Harvesting Antennas*.

Green B.R., Parson W.W. (eds). Dordrecht: Kluwer Academic Publishers, pp. 29–81.
Shi, T., Sun, Y., and Falkowski, P.G. (2007) Effects of iron limitation on the expression of metabolomic genes in the marine cyanobacterium *Trichodesmium erythraeum* IMS101. *Environ Microbiol* **9:** 2945–2956.
Shi, T., Ilikchyan, I., Rabouille, S., and Zehr, J.P. (2010) Genome-wide analysis of diel gene expression in the unicellular N_2-fixing cyanobacterium *Crocosphaera watsonii* WH 8501. *ISME J* **4:** 621–632.
Silva, P., Thompson, E., Bailey, S., Kruse, O., Mullineaux, C.W., Robinson, C., *et al*. (2003) FtsH is involved in the early stages of repair of photosystem II in *Synechocystis* sp PCC 6803. *Plant Cell* **15:** 2152–2164.
Suggett, D.J., Stambler, N., Prasil, O., Kolber, Z., Quigg, A., Vazquez-Dominguez, E., *et al*. (2009) Nitrogen and phosphorus limitation of oceanic microbial growth during spring in the Gulf of Aqaba. *Aquat Microb Ecol* **56:** 227–239.
Tamary, E., Kiss, V., Nevo, R., Adam, Z., Bernát, G., Rexroth, S., Rögner, M., and Reich, Z. (2012) Structural and functional alterations of cyanobacterial phycobilisomes induced by high-light stress. *BBA-Bioenergetics* **1817:** 319–327.
Tuit, C., Waterbury, J., and Ravizza, G. (2004) Diel variation of molybdenum and iron in marine diazotrophic cyanobacteria. *Limnol Oceanogr* **49:** 978–990.
Wegener, K.M., Nagarajan, A., and Pakrasi, H.B. (2014) An atypical psbA gene encodes a sentinel D1 protein to form a physiologically relevant inactive Photosystem II complex in cyanobacteria. *J. Biol. Chem.* **290:** 3764–3774.
Zehr, J.P. (2011) Nitrogen fixation by marine cyanobacteria. *Trends Microbiol* **19:** 162–173.
Zehr, J.P., Bench, S.R., Carter, B.J., Hewson, I., Niazi, F., Shi, T., *et al*. (2008) Globally distributed uncultivated Oceanic N2-fixing Cyanobacteria lack oxygenic photosystem II. *Science* **322:** 1110–1112.
Zehr, J.P., Waterbury, J.B., Turner, P.J., Montoya, J.P., Omoregie, E., Steward, G.F., *et al*. (2001) Unicellular cyanobacteria fix N_2 in the subtropical North Pacific Ocean. *Nature* **412:** 635–638.

Supporting information

Additional Supporting Information may be found in the online version of this article at the publisher's web-site:

Fig. S1. (A) Diel changes in of selected PSI-related parameters of *C. watsonii*. (A) PSI-abundance ($P_{m'max}$) and PSI-mediated putative electron transport ($P_{m'max} \times tg\alpha_{ETR(I)}$) as normalized to Chl level (filled and open circles respectively). (B) Quantum yields of photochemical energy conversion at PSI ($Y(I)$, open squares), and quantum yields of non-photochemical energy dissipation in PSI due to donor side limitation (Y(ND), filled squares). Y(I) and Y(ND) values were derived from steady state (P), maximal (P_m') and zero (P_o) P_{700} levels at the 53 μmol photons m^{-2} s^{-1} step of the corresponding light response curves. The bell shaped dotted lines indicate the diurnal pattern of the growth irradiance. For more details, see Fig. 2 and text.
Fig. S2. 2D CN- and SDS-PAGE of membrane proteins of *C. watsonii* harvested 6 h into the light (6L) and 6 h into the dark (6D) phase. Isolated membrane proteins were labelled with radioactive ^{35}[S]-methionine and separated by CN-PAGE in the first dimension; after which the native gel was photographed (1D colour) and Chl fluorescence (1D fluor) scanned. After SDS-PAGE in the 2nd dimension, the gel was stained by SYPRO Orange (2D SYPRO stain) and electroblotted onto a PVDF membrane, which was dried and exposed to Phosphorimager plate (2D autorads). Complexes are designated as in Figs 6 and 7. Each loaded sample contained 5 μg of Chl.
Fig. S3. Effect of NH_4^+ on the diel cycle of *C. watsonii*. (A) Diel pattern of the maximal PSII quantum yield F_v/F_m in the absence or presence of supplementarily added 0.1 mM NH_4Cl. The arrow at 6L on day 1 shows the time of NH_4Cl addition. The bell shaped dotted lines indicate the diurnal pattern of the growth irradiance. (B) CN gel showing Chl-protein complexes 6 h into the light (6L) and 6 h into the dark (6D) phase after NH_4Cl addition. Complexes are designated as in Figs 6 and 7. Each loaded sample contained 5 μg of Chl.